IEEE Access
Multidisciplinary ⋮ Rapid Review ⋮ Open Access Journal

Received 10 May 2024, accepted 26 May 2024, date of publication 28 May 2024, date of current version 4 June 2024.

Digital Object Identifier 10.1109/ACCESS.2024.3406917

RESEARCH ARTICLE

Self-Supervised Attenuation Method Based on Similarity Comparisons for 3D Seismic Random Noise

JIAN GAO[1], YIXUAN GAO[2], AND WANYUE GAO[3]
[1]School of Earth Science and Technology, China University of Petroleum (East China), Qingdao 266500, China
[2]School of Biological Science, Qufu Normal University, Qufu 273165, China
[3]Business School, Shandong Normal University, Jinan 250358, China

Corresponding author: Jian Gao (1946595208@qq.com)

ABSTRACT The improvement of the signal-to-noise ratio of seismic data is crucial for high-precision processing. The self-supervised denoising methods based on correlation differences are gaining attention due to their low cost of training data construction and the ability to build training data directly on test data. However, as the volume of data processed increases, these methods must maintain a denoising effect by adding extra processings. This increase in processing times can lead to a rise in total cost, making these methods less cost-effective compared to other deep learning methods for processing large data. Therefore, we improved these self-supervised methods by altering the training data construction process, thereby retaining its cost advantage. Specifically, we modified the selection process of zones used for training data construction. Through correlation analysis, these methods can obtain higher-quality zones from the original zone for training, indicating that the network needs to be trained only once to process any data in the original zone. Without the requirement for additional processing to ensure noise attenuation, these self-supervised methods can maintain their cost advantage when processing large data. We applied one of these self-supervised methods to synthetic and field examples to demonstrate the enhancement's effectiveness. Experimental results show that the improved method performs as well as the conventional self-supervised method in suppressing random noise and constructing reflection events but with a significant cost advantage.

INDEX TERMS Seismic data, random noise, deep learning, noise attenuation.

I. INTRODUCTION

The significance of precise geological exploration is becoming more apparent with the increasing focus on deep and ultra-deep seismic exploration. High-precision seismic exploration necessitates seismic data with a high signal-to-noise ratio (SNR) to ensure accurate seismic data inversion and geological interpretation [1]. During the seismic data acquisition process, noise inevitably contaminates the data. There are two types of noise: coherent noise and random noise. Coherent noise has a fixed frequency and apparent velocity, whereas random noise is typically caused by various disturbances in the acquisition environment and has no fixed frequency or apparent velocity. Random noise can significantly reduce the SNR of seismic data and affect subsequent processing of the seismic data. The attenuation of random noise in seismic data has consequently received considerable attention from researchers.

Various methods have been proposed to reduce random noise in seismic data. Prediction filtering methods [2], [3], [4], [5] assume that effective seismic signals can be predicted in the frequency or time domain, whereas random noise remains unpredictable. Appropriate filter operators can be designed to reduce random noise in the frequency domain based on this difference in predictive characteristics. A subsequent inverse transformation can then be used to obtain clean

The associate editor coordinating the review of this manuscript and approving it for publication was Geng-Ming Jiang.

data. Transform-domain filtering approaches [6], [7], [8], [9] can convert seismic data to a specified transform domain and then apply specific thresholds to perform denoising. These thresholds are formulated based on the distinguishable difference between effective signals and random noise within the transform coefficients. While effective at attenuating random noise, these transform-domain methods often fail to completely eliminate noise. This is because these methods often blend a mixture of noise and valid data, resulting in residual noise. Modal decomposition methods [10], [11], [12], [13] aim to improve signal reconstruction and reduce random noise by decomposing seismic data into multiple components and superimposing primary components representing clean data. However, the clean data and noise can be inevitablely mixed during this decomposition process. This can result in multiple signal components with indeterminate mixing ratios, potentially leading to loss of effective signal and residual noise in the denoised output. Rank-reduction methods [14], [15], [16], [17], such as multichannel singular value analysis (MSSA), propose that the optimal clean data can be represented as a low-rank matrix. The target is to attenuate the rank enhancement induced by the random noise present in the seismic signal matrix, thereby facilitating noise suppression. Machine learning methods, with their innovative and efficient approach to data processing tasks, have gained considerable traction. Among these, techniques based on deep learning, especially those using convolutional networks, have made significant progress. Numerous deep learning-based methods [18], [19], [20], [21], [22], [23], [24], [25] have also been proposed for seismic denoising, especially for suppressing random noise. These techniques have significantly improved SNR of seismic data and attenuated random noise. However, the complexity and diversity of geological structures pose a challenge for deep learning methods, making it difficult to process all data with a universal training dataset. Typically, most methods can only reference the geological structure and features of the test area to construct training datasets with similar features, which complicates data processing to some extent.

In recent years, self-supervised denoising methods [18], [26], [27] based on similarity differences have gained attention. Unlike other deep learning methods, which require referencing geological features of the test zone to build a training dataset, these self-supervised methods can construct a training dataset directly from the test zone. This significantly reduces the cost of training data construction. However, as the volume of data processed increases, the cost advantage becomes less evident. This is due to the additional processing required by self-supervised methods on large data processing, which increases the overall cost. Specifically, these methods need to divide the large original data into several test data and process them independently. This strategy ensures differences in network learning rates between clean data and random noise in each test data, thereby effectively ensuring the effect of noise attenuation on the large original data.

Therefore, we proposed an improved self-supervised suppression method based on correlation differences. This improved method primarily alters the selection process of zones used for constructing training data. By performing correlation analysis between each selected zone, it can select zones with less similarity, thus building a higher-quality training dataset. With this high-quality dataset, this method eliminates the need to divide the large original data into several test data and process them individually. It only needs to be trained once to process any data in the large original data. In addition, this improved method has a similar training calculation cost to the conventional self-supervised method. Specifically, the training calculation cost for the improved method on large original data is similar to the cost for the conventional method on single test data. These advantages in cost lead to a significant reduction in the total cost for processing the entire large data. Moreover, complex geological structures usually represent only a small portion of the overall data. This ratio is also reflected in the training data when using conventional self-supervised methods. Consequently, these methods may perform worse when processing complex structures compared to their performances on more common and relatively simple structures. However, with high-quality zone selection, self-supervised methods can more easily capture zones with complex structures. It increases the ratio of data representing these structures in the training dataset, leading to improved performance when processing complex structures.

The rest of this paper is organized as follows. Section II presents the denoising strategy of a self-supervised method we used for the test, the corresponding specific approaches of the conventional method and the improved method, and similarity analysis. Section III introduces the network we applied in this paper. In Section IV, experiments are conducted on synthetic and field data to demonstrate the effectiveness of the improved method in attenuating random noise and reducing the cost of processing. Finally, Section V concludes this paper.

II. METHODS

Conventional self-supervised methods employ various strategies to achieve similarity differences between valid data and random noise for noise attention. For comparison purposes, we used one such conventional method (MRN-OLD) [26] for the test. Fig. 1(a) and Fig. 1(b) illustrate the processing flow of the original zone using the improved method and the conventional method, respectively. Despite differences in their zone selection processes, both methods apply the same denoising strategy.

A. DENOISING STRATEGY BASED ON DIVISION

As we know, 3D seismic data ($Y_{m,n,t}$) can be expressed as follows:

$$Y_{m,n,t} = X_{m,n,t} + noise_{m,n,t} \tag{1}$$

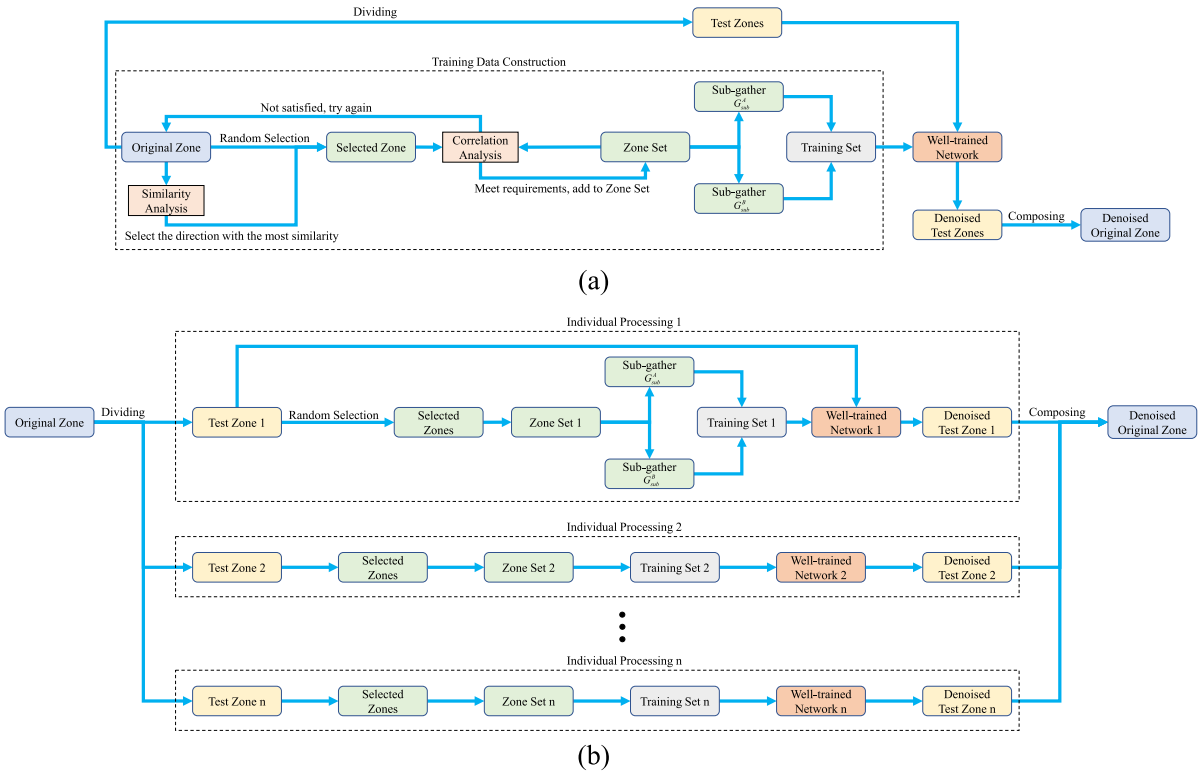

FIGURE 1. Flows of self-supervised methods for 3D seismic random noise attenuation. (a) The improved method (MRN-NEW). (b) Conventional self-supervised method for comparison (MRN-OLD).

where $X_{m,n,t}$ denotes clean data; $noise_{m,n,t}$ denotes Gaussian white noise; m and n denote trace number; and t denotes time sampling point. Clean data in adjacent traces generally show similar seismic characteristics, such as interface and phase, indicating spatial correlation. On the other hand, random noise, being a disorganized time series, lacks spatial correlation. Thus, the similarity of clean data and random noise between adjacent traces can be described as follows:

$$\begin{cases} X_{2m-1,n,t} \approx X_{2m,n,t} \\ noise_{2m-1,n,t} \neq noise_{2m,n,t} \end{cases}. \tag{2}$$

The difference in similarity between clean data and random noise can affect the network's learning efficiency towards both, subsequently leading to a difference in the network's mastery of the two.

$$\begin{aligned} &Diff_{sim}\left(X_{m,n,t}, noise_{m,n,t}\right) \\ &\Downarrow \\ &Diff_{le}\left(X_{m,n,t}, noise_{m,n,t}\right) \\ &\Downarrow \\ &Diff_{mas}\left(X_{m,n,t}, noise_{m,n,t}\right) \end{aligned} \tag{3}$$

where $Diff_{sim}$, $Diff_{le}$, and $Diff_{mas}$ denote the difference in similarity, learning efficiency of network, and mastery of network, respectively. Specifically, an increased similarity can reduce the complexity of network learning, thereby enhancing its efficiency. Consequently, given the same timeframe, a network can learn clean data more swiftly than random noise. Furthermore, according to Gao et al. theory [26], the network parameter vector can be significantly influenced by a specific local optimal solution with a denoising effect during the initial training epochs due to the statistical characteristics of random noise. If the parameter vector is located near this specific optimal solution, the corresponding model can exhibit noise attenuation.

Therefore, by dividing the original gather into two sub-gathers (G^A_{sub} and G^B_{sub}) based on the trace number's parity, and using them as the network's input and label respectively, we can find an appropriate epoch interval ($[E_{min}, E_{max}]$). In this epoch interval, the corresponding model ($F_{Net}(:;\varphi), \varphi \in [E_{min}, E_{max}]$) can achieve noise attenuation and signal reconstruction effectively.

$$F_{Net}\left(Y_{m,n,t};\varphi\right) = F_{Net}\left(X_{m,n,t} + noise_{m,n,t};\varphi\right) \approx X_{m,n,t} \tag{4}$$

The mean square error (MSE) is commonly employed to assess the network's training efficiency. The loss function in this article can be expressed as follows:

$$L(\theta) = \frac{1}{2M}\sum_{i=1}^{M}\left\|F_{Net}\left(B_i^I;\theta\right) - B_i^L\right\|_F^2 \tag{5}$$

where M represents the number of samples in the training set; $\|\cdot\|_F$ represents the Frobenius norm; B_i^I denotes the patches from the input; B_i^L denotes those from the label.

B. CONVENTIONAL SELF-SUPERVISED METHOD

The flow of conventional self-supervised method (MRN-OLD) for processing an original zone is shown in Fig.1 (b). The process can be described in detail as follows.

Step 1: Divide several appropriate test zones from the original zone.

Step 2: Process each test zone individually. For each test zone, randomly select small zones from the test zone to be the selected zones, and add them to the zone set. Then, divide the zones from the zone set into two sub-gathers (G_{sub}^A and G_{sub}^B) based on the parity of the trace number. Next, utilize these two sub-gathers to construct the training data.

Step 3: Obtain well-trained networks from each training data. Then perform noise attenuation on each test zone by corresponding well-trained network.

Step 4: Compose denoised test zones into denoised original zone.

Random selection of zones in this method can enhance data diversity in the selected zones, thereby improving data quality. However, as the test zone size increases, ensuring this diversity becomes challenging, and the selection loss of complex structures is inevitable. Furthermore, a larger test zone can reduce the learning efficiency difference between clean data and random noise in the network. This could potentially lead to a failure in obtaining a model with a noise attenuation effect. Therefore, it is necessary for conventional self-supervised method to divide large original zone into several small test zones and perform individual processings to ensure the effect of noise attenuation. However, it can increase the total cost for processing the large data due to these additional processings.

C. THE IMPROVED METHOD

The flow of the improved method (MRN-NEW) for processing original zone is shown in Fig.1 (a). The process can be described in detail as follows.

Step 1: Identify the direction with the highest similarity in the 3D original zone. Given the random distribution and limited power of random noise, the similarity between adjacent seismic traces primarily reflects the similarity of effective data. Hence, the greater the similarity between adjacent seismic traces, the larger the difference in learning efficiency between clean data and random noise.

Step 2: Select small zones from the original zone randomly. After the first selected zone is directly added to the zone set, each subsequent selected zone must undergo a similarity analysis (correlation analysis) with every zone in the zone set. Only zones that meet the similarity requirements with all zones in the zone set can be added to the zone set.

Step 3: Repeat Step 2 until the demand for the number of training samples is satisfied.

Step 4: Divide the zones from the zone set into two sub-gathers (G_{sub}^A and G_{sub}^B) based on the parity of the trace number. Then, utilize these two sub-gathers to construct the training data.

Step 5: Obtain well-trained network from the training data. Then perform noise attenuation on each test zone by the well-trained network.

Step 6: Compose denoised test zones into denoised original zone.

Compared to the conventional self-supervised method (MRN-OLD), the improved method doesn't need to consider the influence of the test zone size. On the one hand, the improved method can easily identify complex structures to construct high-quality training data through similarity analysis. On the other hand, with this high-quality training data and a limited number of training samples, the difference in learning efficiency can be easily guaranteed. Therefore, it's unnecessary to divide the original zone into smaller test zones and perform independent processings to ensure noise attenuation. With the improved method, the network needs to be trained only once to perform noise attenuation anywhere in the original zone.

D. SIMILARITY ANALYSIS

The Structural Similarity Index Measure (SSIM) can be used for similarity analysis. SSIM is a perceptual model which quantifies image distortion and measures the similarity between two images. It evaluates images based on three aspects: luminance, contrast, and structure. We used SSIM and a threshold a to determine the similarity between the two zones. If the SSIM value is less than or equal to the threshold a, it suggests that the selected zone satisfies the similarity requirement with the reference zone. In this article, we set the threshold a at 0.4.

III. NETWORK ARCHITECTURE

In this article, we employed M-ResUNet [26] to demonstrate the effectiveness of our improved methodology, as depicted in Fig. 2(a). Unlike the traditional U-shaped pathway of the conventional UNet network, M-ResUNet performs additional processings on certain feature maps for improved training results. The M-ResUNet network consists of three core structures: the U-shaped structure, the feature enhancement structure, and the multi-layer descending structure.

The U-shaped structure extracts features at different levels and provides an interface for further feature processing. The feature enhancement structure can process features with a specific scale and control the bias of the final output towards various scale features by adjusting the ratio of the channels associated with these features. Lastly, the multi-layer descending structure minimizes feature loss after convolution operations and possesses a larger count and a wider selection space for parameters, thereby accelerating network learning.

Additionally, a feature processing module, comprised of two components, Conv Block A and Conv Block B, is utilized

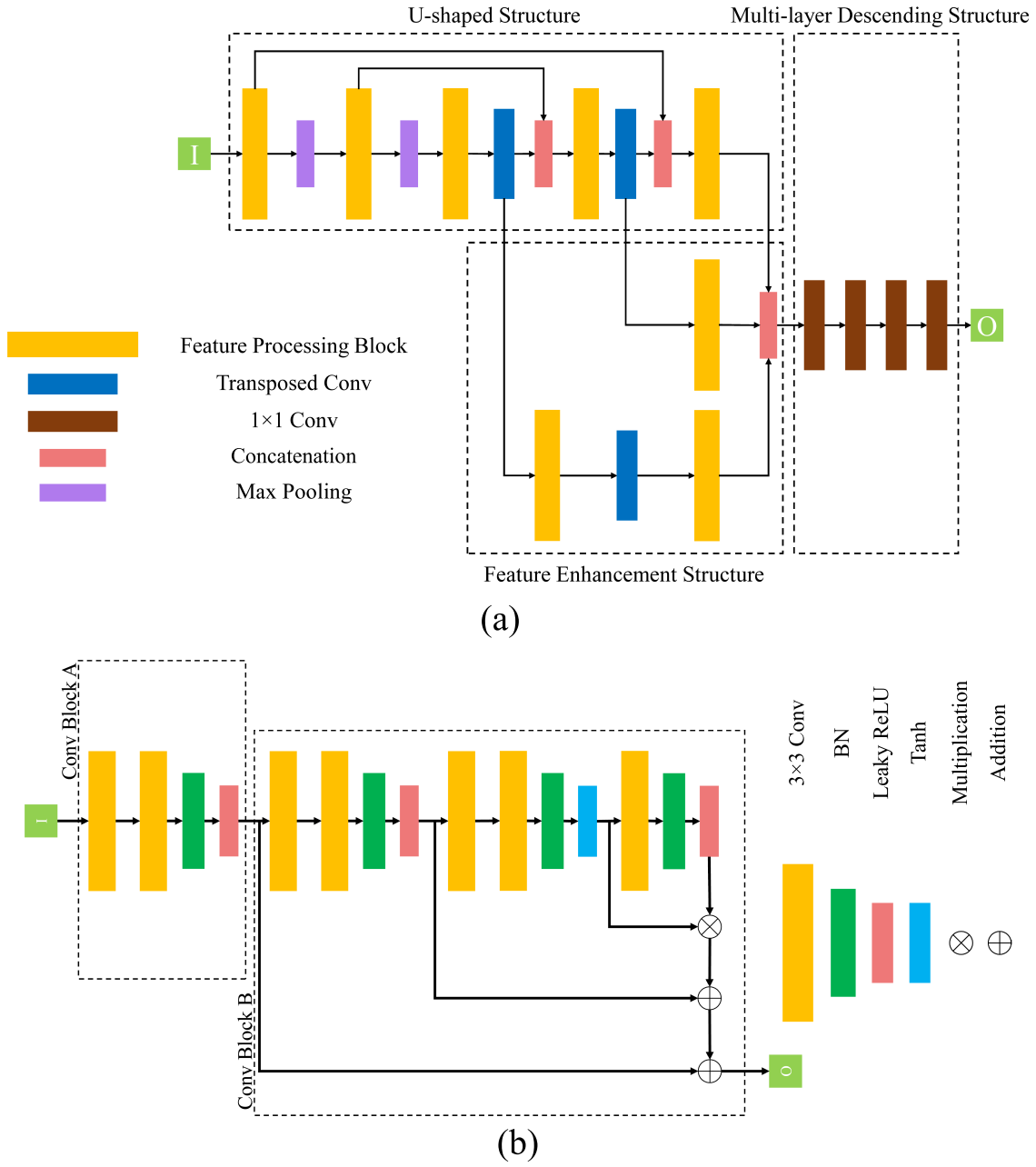

FIGURE 2. M-ResUNet framework. (a) Overall framework. (b) Feature processing module.

to enhance network learning, as illustrated in Fig. 2(b). Conv Block A facilitates feature extraction across all data through consecutive double convolutions. In contrast, Conv Block B hastens the update of the network parameter vector towards the specific local optimal solution with a denoising effect through a unique multiple residual structure.

IV. NUMERICAL RESULTS

In this section, we performed experiments on synthetic and field examples to demonstrate the effectiveness of the improved method. However, it is challenging to evaluate its effect directly on original zone processing, as the way of dividing on original zone has an obvious influence on the total cost. To further compare the total cost between methods, we used the calculation cost for a single test zone to estimate the cost for the whole original zone, which can eliminate the influence of dividing and effectively assess the cost. In addition, all experiments were performed on a PC (Intel Core i5-12400F 2.50 GHz CPU, 16-GB memory, and an NVIDIA GeForce RTX 3060 GPU).

A. DATA ANALYSIS

To quantitatively assess the denoising performance from different methods, the SNR and root mean squared

TABLE 1. Training information of network for examples.

Information	Synthetic example	First field example	Second field example
Solver	Adam	Adam	Adam
Initial learning rate	0.001	0.001	0.001
Patch size	20×20×20	20×20×20	20×20×20
Batch size	32	32	32
Training epoch	12	6	18
Sample number	192	640	192

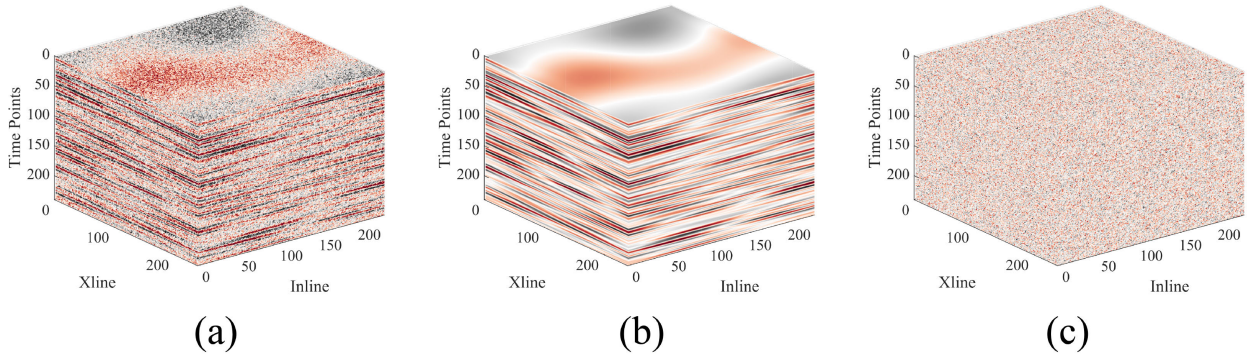

FIGURE 3. Synthetic original zone for training. (a) Noisy data. (b) Clean data. (c) Random noise.

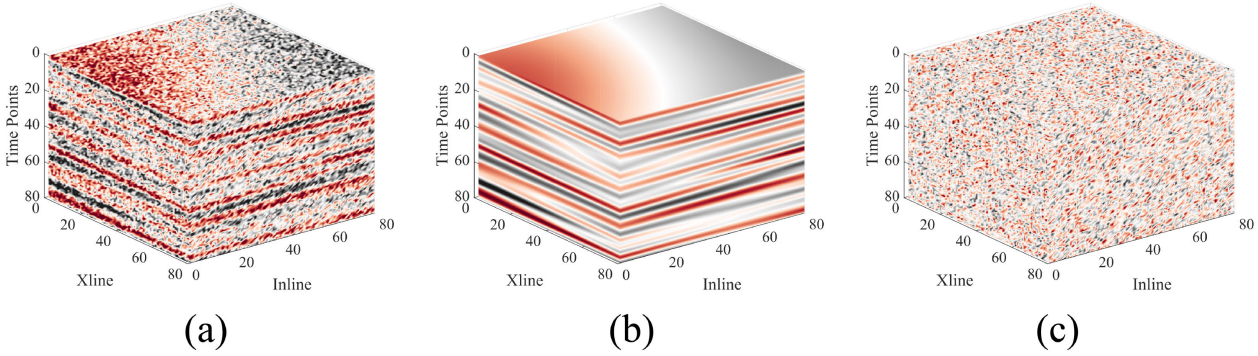

FIGURE 4. Synthetic example for test. (a) Noisy data. (b) Clean data. (c) Random noise.

error (RMSE) [28] were applied to evaluate the results. SNR and RMSE can be expressed as follows:

$$SNR = 10\log_{10}\left(\frac{\sum_{i=1}^{N}\sum_{j=1}^{M}\sum_{k=1}^{L}\left(X_{i,j,k}\right)^2}{\sum_{i=1}^{N}\sum_{j=1}^{M}\sum_{k=1}^{L}\left(F_{Net}\left(Y_{i,j,k}\right)-X_{i,j,k}\right)^2}\right) \tag{6}$$

$$RMSE = \sqrt{\frac{1}{NML}\sum_{i=1}^{N}\sum_{j=1}^{M}\sum_{k=1}^{L}\left(F_{Net}\left(Y_{i,j,k}\right)-X_{i,j,k}\right)^2} \tag{7}$$

where $F_{Net}\left(Y_{i,j,k}\right)$ and $X_{i,j,k}$ represent the denoising result and the clean data, respectively; M, N, and L are the dimensions of the seismic data. In addition, to provide a more accurate assessment of the total computational cost for the original zone, we have established a new evaluation index, that is pixel number per second for processing (*PNS*), as follows:

$$PNS = \frac{S}{T_{prep} + T_{train} + T_{proc}} \tag{8}$$

where T_{prep} denotes preparation time for training data construction; T_{train} denotes training time; T_{proc} denotes processing time for data; S denotes the number of pixel in the zone for processing. Due to differences in processing ways between MRN-NEW and MRN-OLD, the *PNS* needs minor adjustments.

MRN-OLD requires individual processing on each test zone, that is MRN-OLD needs to perform independent training dataset construction, training, and processing for each test zone. Thus, *PNS* of MRN-OLD for a test zone can be approximately regarded as *PNS* for the original zone. The

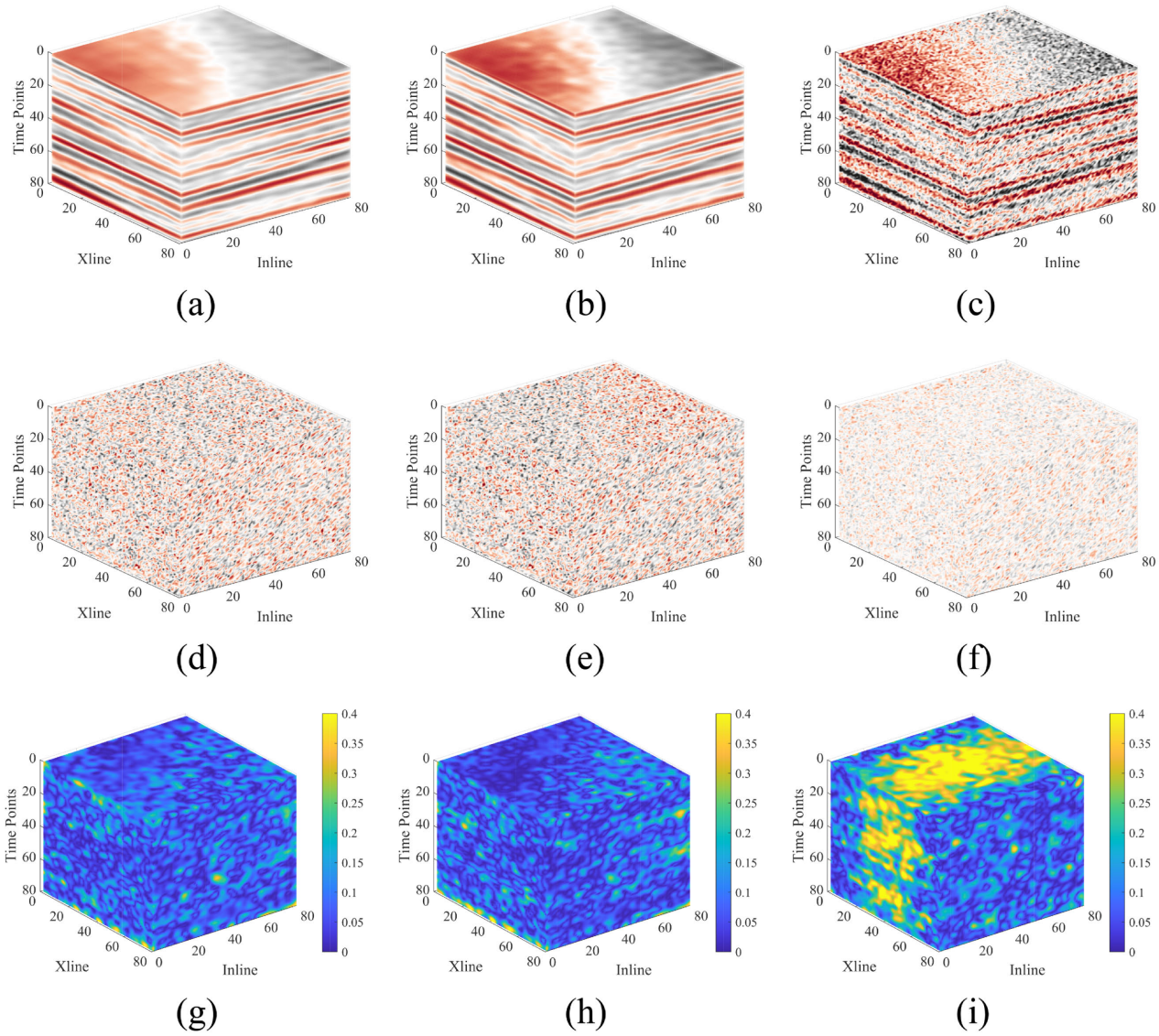

FIGURE 5. Denoising performances of synthetic example. (a)-(c) Denoising results: MRN-NEW, MRN-OLD, and MSSA. (d)-(f) Removed noise: MRN-NEW, MRN-OLD, and MSSA. (g)-(i) Local similarity maps: MRN-NEW, MRN-OLD, and MSSA.

PNS of MRN-OLD (PNS_{OLD}) is as follows:

$$PNS_{OLD} = \frac{S^{test}}{T^{test}_{prep} + T^{test}_{train} + T^{test}_{proc}} \tag{9}$$

where T^{test}_{prep}, T^{test}_{train}, T^{test}_{proc} and S^{test} denote the T_{prep}, T_{train}, T_{proc} and S of the test zone. Since MRN-NEW only needs to be trained once to process any test data within the original zone, its *PNS* for the original zone (PNS_{NEW}) can be as follows:

$$PNS_{NEW} = \frac{S^{orig}}{T^{orig}_{prep} + T^{orig}_{train} + \frac{S^{orig}}{S^{test}} T^{test}_{proc}} \tag{10}$$

where T^{orig}_{prep}, T^{orig}_{train} and S^{orig} denote the T_{prep}, T_{train} and S of the original zone. The T_{proc} for original zone can be approximately regarded as $\frac{S^{orig}}{S^{test}} T^{test}_{proc}$.

B. NETWORK TRAINING SETTINGS

In this article, we used the conventional self-supervised method from Gao et al. (MRN-OLD) for comparison, as seen in Fig. 1(b). As shown in Table 1, most of hyperparameters for the improved method (MRN-NEW) are identical to those of MRN-OLD. Both methods use the Adam optimizer with an initial learning rate of 0.001. The patch size is set to 20×20×20, and the batch size is set to 32. The training set for the synthetic example had 192 samples, while the set for the field examples contained 640 samples and 192 samples, respectively. We conducted training for the synthetic example to 12 epochs and for the two field examples to 6 epochs and 18 epochs, respectively. It's worth noting that the training zone for MRN-NEW covers the entire original zone. This means it only needs to be trained once to process any zone

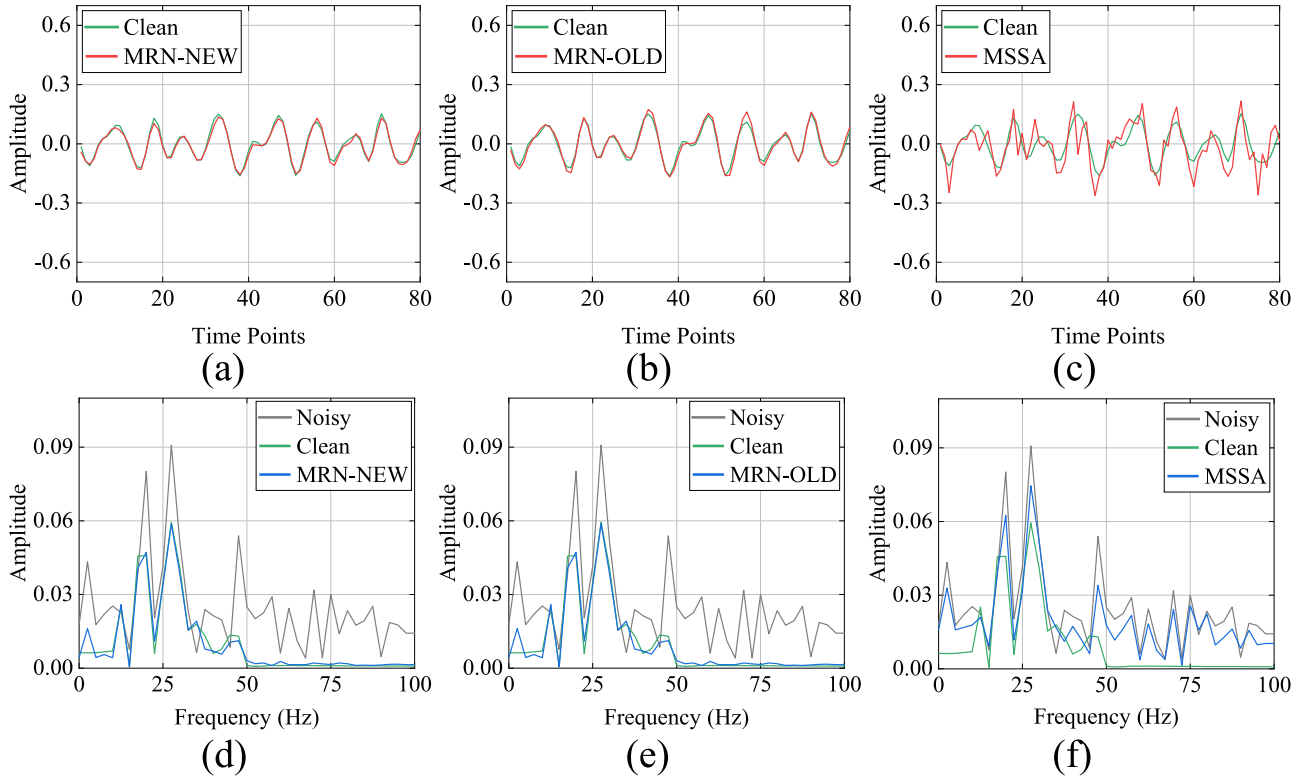

FIGURE 6. Amplitude comparisons and spectrum comparisons on a trace record (Xline=40, Inline=40). (a)-(c) Amplitude comparisons: MRN-NEW, MRN-OLD, and MSSA. (d)-(f) Spectrum comparisons: MRN-NEW, MRN-OLD, and MSSA.

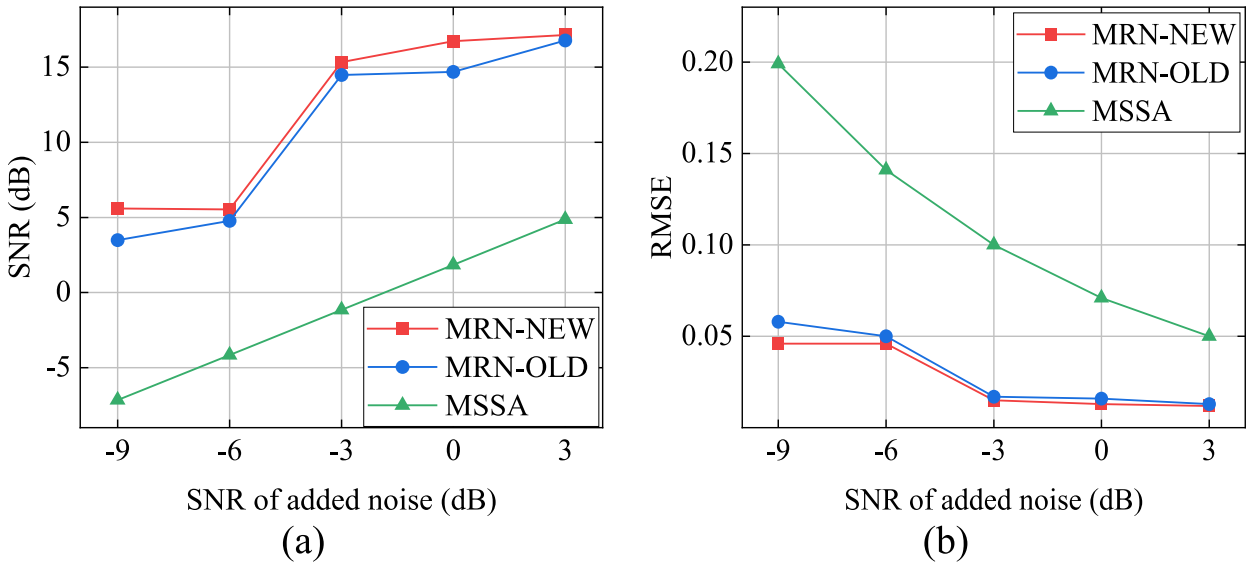

FIGURE 7. SNR and RMSE comparisons at different noise levels. (a) SNR comparison. (b) RMSE comparison.

inside the original zone. However, MRN-OLD's training zone is limited to its test zone.

C. EXPERIMENTS ON SYNTHETIC DATA

To showcase the outstanding performance of our improved method, we chose synthetic post-stack data with a 240×240×240 zone as the original zone. From this, we selected an 80×80×80 zone to serve as our test zone. We added 0dB of random noise to the original zone to create a synthetic example, as displayed in Fig. 3. Fig. 4(a)-(c) illustrate the noisy data, clean data, and added noise within the test zone. The denoising results

TABLE 2. Computational cost comparisons for synthetic example.

Information	MRN-NEW	MRN-OLD
Preparation time T_{prep} (s)	104.43	0.85
Training time T_{train} (s)	140	141
Processing time T_{proc} (s)	156.06	5.24
Pixel number S	13,824,000	512,000
PNS	34,517.72	3,480.86

TABLE 3. SNR and RMSE of the Synthetic Results [SNR (dB)/RMSE].

Added Noise (dB)	MRN-NEW	MRN-OLD	MSSA
-9	5.588/0.046	3.483/0.058	-7.162/0.199
-6	5.526/0.046	4.770/0.050	-4.160/0.141
-3	15.338/0.015	14.477/0.017	-1.158/0.100
0	16.729/0.013	14.686/0.016	1.844/0.071
3	17.151/0.012	16.788/0.013	4.859/0.050

for MRN-NEW, MRN-OLD, and MSSA are displayed in Fig. 5(a)-(c), with respective SNRs of 16.729 dB, 14.686 dB, and 1.844 dB. Both MRN-NEW and MRN-OLD perform well in attenuating noise, whereas MSSA remains obvious residual noise. The corresponding removed noises and local similarity maps can be viewed in Fig. 5(d)-(f) and Fig. 5(g)-(i). MRN-NEW and MRN-OLD show similar performance in amplitude preservation, both outperforming MSSA. The comparisons of computational costs for self-supervised methods are presented in the Table 2. Note that the processing time of MRN-NEW represents the time cost for the original zone, which is converted from the processing time of the test zone. The *PNS* for MRN-NEW is 34,517.72, while the *PNS* for MRN-OLD is 3,480.86. The processing efficiency of MRN-NEW is approximately 10 times that of MRN-OLD. Despite requiring more time for training data construction, training, and processing, MRN-NEW significantly outperforms MRN-OLD. This improvement in processing efficiency is due to the much larger number of pixels processed by MRN-NEW.

Moreover, we performed comparisons of amplitude and spectrum on a specific trace record (Xline=40, Inline=40), depicted in Fig. 6. It's evident that MRN-NEW and MRN-OLD display similar efficiency in noise attenuation, surpassing MSSA. Lastly, we applied these methods to a synthetic example with five different levels of random noise. We compared their SNRs and RMSEs, as shown in Fig. 7 and Table 3. The results show that MRN-NEW generally outperforms MRN-OLD across different noise levels, demonstrating superior resistance to strong noise interference.

D. EXPERIMENTS ON FIELD DATA

To further demonstrate the effectiveness of our improved method, we first utilized post-stack field data from an original zone measuring 1252×734×286 for the test. We selected a 240×240×240 zone from the original zone as our test zone, as shown in Fig. 8. Fig. 9(a)-(c) present the denoising results for MRN-NEW, MRN-OLD, and MSSA. Both MRN-NEW and MRN-OLD effectively attenuate noise, whereas MSSA leaves noticeable residual noise. The corresponding removed noises and local similarity maps are shown in Fig. 9(d)-(f) and Fig. 9(g)-(i). MRN-NEW and MRN-OLD exhibit similar performance in amplitude preservation, both surpassing MSSA. Table 4 presents the cost comparisons of self-supervised methods for the first field example. The *PNS* for MRN-NEW is 72,298.38, while the *PNS* for MRN-OLD is 34,742.40. The processing efficiency of MRN-NEW is approximately 2 times that of MRN-OLD. As the test zone expands, the number of samples in the test set that need processing gradually increases. This results in a notable rise in the cost of single, independent processing, while the cost associated with the number of times for independent processing becomes less significant. Even though the processing efficiency advantage of MRN-NEW has diminished in this example, it still outperforms MRN-OLD.

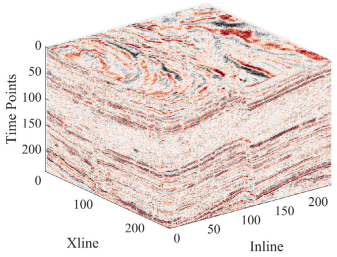

FIGURE 8. First field example for test.

TABLE 4. Computational cost comparisons for first field example.

Information	MRN-NEW	MRN-OLD
Preparation time T_{prep} (s)	162.27	1.64
Training time T_{train} (s)	224	219
Processing time T_{proc} (s)	3,248.81	177.26
Pixel number S	262,824,848	13,824,000
PNS	72,298.38	34,742.40

TABLE 5. Computational cost comparisons for second field example.

Information	MRN-NEW	MRN-OLD
Preparation time T_{prep} (s)	271.10	3.64
Training time T_{train} (s)	216	218
Processing time T_{proc} (s)	15,669.45	5.50
Pixel number S	1,485,696,000	512,000
PNS	91,956.27	2,254.12

Furthermore, we used additional post-stack field data from an original zone measuring 1500 × 3392x292 for testing. We chose an 80 × 80x80 zone from the original zone as our test zone, as shown in Fig. 10. Fig. 11(a)-(c) displays the denoising results for MRN-NEW, MRN-OLD, and MSSA. All methods effectively attenuate random noise, but both MRN-NEW and MRN-OLD outperform MSSA in maintaining the continuity of reflection events. The removed noises and local similarity maps are shown in Fig. 11(d)-(f) and Fig. 11(g)-(i). MSSA preserves more clear reflection events in its removed noise than MRN-NEW and MRN-OLD. Additionally, MSSA exhibits higher similarity in

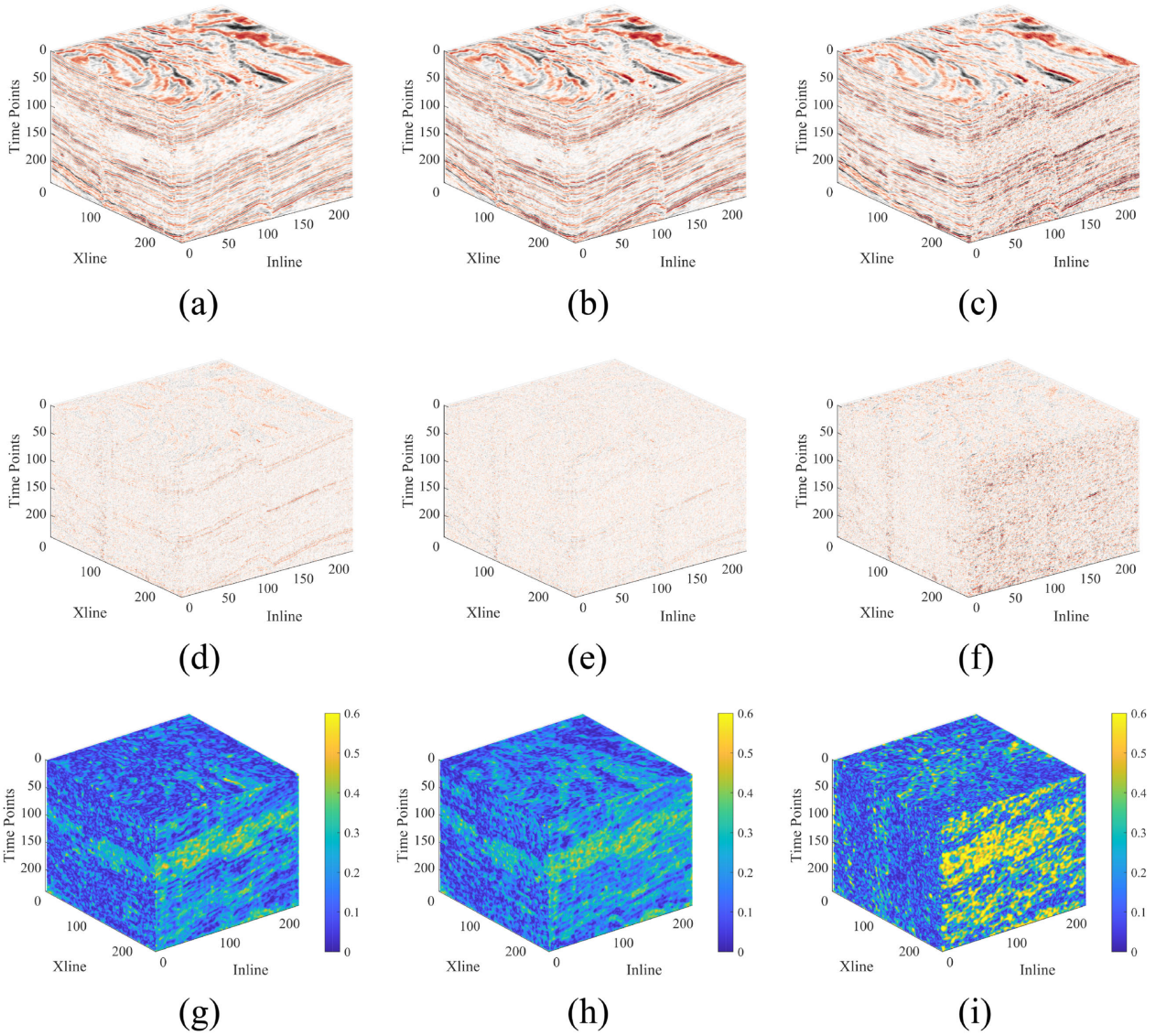

FIGURE 9. Denoising performances for first field example. (a)-(c) Denoising results: MRN-NEW, MRN-OLD, and MSSA. (d)-(f) Removed noise: MRN-NEW, MRN-OLD, and MSSA. (g)-(i) Local similarity maps: MRN-NEW, MRN-OLD, and MSSA.

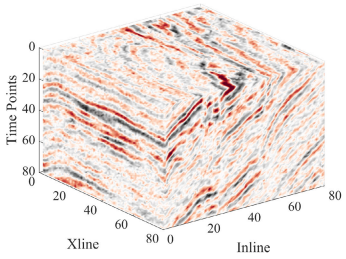

FIGURE 10. Second field example for test.

its local similarity map compared to MRN-NEW and MRN-OLD. Therefore, it's evident that MSSA performs the poorest in amplitude preservation. MRN-NEW slightly outperforms MRN-OLD in amplitude preservation due to its slightly lower similarity in its local similarity map. Table 5 presents the cost comparisons of self-supervised methods for the second field example. The *PNS* for MRN-NEW is 91,956.27, while the *PNS* for MRN-OLD is 2,254.12. The processing efficiency of MRN-NEW is approximately 41 times that of MRN-OLD. As the original zone expands and the test zone shrinks, the cost of single independent processing is no longer significant, while the cost associated with the number of times for independent processing increases significantly. In this example, the processing efficiency advantage of MRN-NEW is significantly better than that of MRN-OLD. Considering that the size of the test zone cannot be infinitely increased and the massive amount of data needs to be processed, the cost comparison of this example still has a certain reference value.

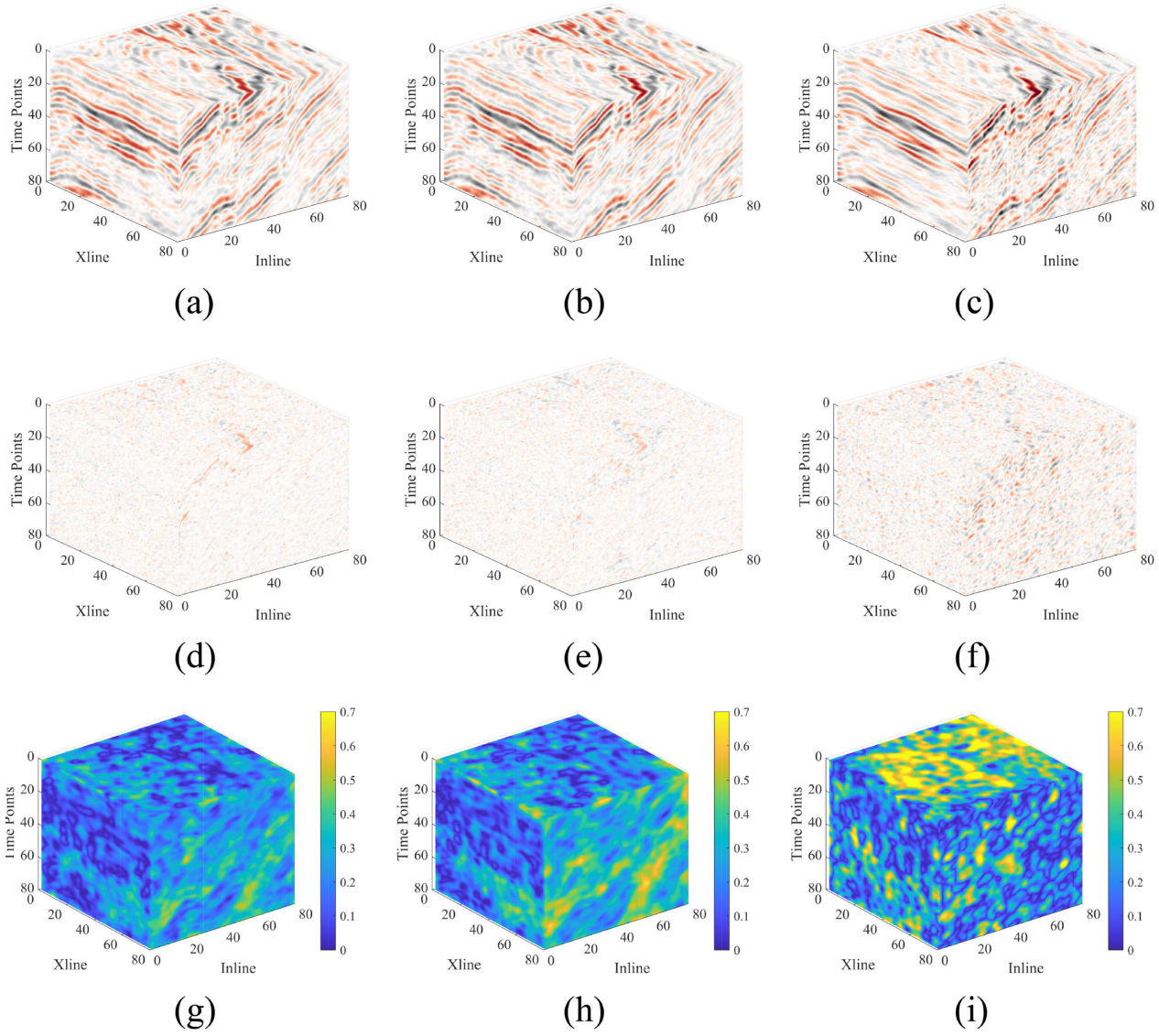

FIGURE 11. Denoising performances for second field example. (a)-(c) Denoising results: MRN-NEW, MRN-OLD, and MSSA. (d)-(f) Removed noise: MRN-NEW, MRN-OLD, and MSSA. (g)-(i) Local similarity maps: MRN-NEW, MRN-OLD, and MSSA.

V. CONCLUSION

In this article, we address the cost challenge of self-supervised attenuation methods for random noise in large-volume 3D seismic data. We improved the zone selection process for self-supervised methods, facilitating the selection of higher-quality zones. With this high-quality dataset, the network only needs to be trained once to process any data in the original zone. This eliminates the need for conventional self-supervised methods to perform independent processing on large data. It effectively reduces the influence of the cost caused by the number of times for independent processing, thereby maintaining the total cost advantage of self-supervised methods when they process large data. Experimental evaluations using synthetic and field data have demonstrated the improved method's excellent performance in random noise attenuation and total cost reduction. However, under very low SNR conditions, the method's denoising ability may be compromised. Furthermore, a method for quickly selecting the SSIM value and training sample number for large 3D data needs to be explored. This is because different original zones with varying sizes, resolutions, and structural complexities lead to differences in the suitable value of SSIM and the number of training samples. Selecting the wrong SSIM value or training sample number can increase the calculation cost and make the improved method more difficult to use. Despite these limitations, our improved method shows promise in complex random noise attenuation and cost reduction.

ACKNOWLEDGMENT

The authors would like to thank the reviewers and the journal's editors. Comments by the journal's editors and the associated reviewers are very helpful in improving the manuscript.

REFERENCES

[1] S. M. Mousavi and G. C. Beroza, "Deep-learning seismology," *Science*, vol. 377, no. 6607, 2022, Art. no. eabm4470.
[2] G. Liu, X. Chen, J. Du, and K. Wu, "Random noise attenuation using f-x regularized nonstationary autoregression," *Geophysics*, vol. 77, no. 2, pp. 61–69, Mar. 2012.
[3] D. Bonar and M. Sacchi, "Spectral decomposition with f-x-y preconditioning," *Geophys. Prospecting*, vol. 61, pp. 152–165, Jun. 2013.
[4] M. Bagheri, M. A. Riahi, and H. Hashemi, "Denoising and improving the quality of seismic data using combination of DBM filter and FX deconvolution," *Arabian J. Geosci.*, vol. 10, no. 19, pp. 1–8, Oct. 2017.
[5] K. Chen and M. D. Sacchi, "Robust f-x projection filtering for simultaneous random and erratic seismic noise attenuation," *Geophys. Prospecting*, vol. 65, no. 3, pp. 650–668, 2017.
[6] H. Shan, J. Ma, and H. Yang, "Comparisons of wavelets, contourlets and curvelets in seismic denoising," *J. Appl. Geophys.*, vol. 69, no. 2, pp. 103–115, 2009.
[7] Z. Yu and D. Whitcombe, "Seismic noise attenuation using 2D complex wavelet transform," in *Proc. 70th Annu. Int. Conf. Exhib.*, vol. 15, 2008, p. cp-40-00232.
[8] N. Liu, Y. Yang, Z. Li, J. Gao, X. Jiang, and S. Pan, "Seismic signal denoising using time–frequency peak filtering based on empirical wavelet transform," *Acta Geophysica*, vol. 68, pp. 425–434, Apr. 2020.
[9] S.-A. Ouadfeul and L. Aliouane, "Random seismic noise attenuation data using the discrete and the continuous wavelet transforms," *Arabian J. Geosci.*, vol. 7, pp. 2531–2537, Jul. 2014.
[10] W. Liu, Y. Liu, S. Li, and Y. Chen, "A review of variational mode decomposition in seismic data analysis," *Surv. Geophys.*, vol. 44, no. 2, pp. 323–355, 2023.
[11] F. Li, B. Zhang, S. Verma, and K. J. Marfurt, "Seismic signal denoising using thresholded variational mode decomposition," *Explor. Geophys.*, vol. 49, no. 4, pp. 450–461, Aug. 2018.
[12] T. P. Banjade, S. Yu, and J. Ma, "Earthquake accelerogram denoising by wavelet-based variational mode decomposition," *J. Seismol.*, vol. 23, no. 4, pp. 649–663, Jul. 2019.
[13] J. Feng, X. Liu, X. Li, W. Xu, and B. Liu, "Low-rank tensor minimization method for seismic denoising based on variational mode decomposition," *IEEE Geosci. Remote Sens. Lett.*, vol. 19, pp. 1–5, 2022.
[14] D. Zhang, Y. Chen, W. Huang, and S. Gan, "Multi-step damped multichannel singular spectrum analysis for simultaneous reconstruction and denoising of 3D seismic data," *J. Geophys. Eng.*, vol. 13, no. 5, pp. 704–721, 2016.
[15] Y. Zhang, H. Zhang, Y. Yang, N. Liu, and J. Gao, "Seismic random noise separation and attenuation based on MVMD and MSSA," *IEEE Trans. Geosci. Remote Sens.*, vol. 60, pp. 1–16, 2022, Art. no. 5908916.
[16] V. Oropeza and M. Sacchi, "Simultaneous seismic data denoising and reconstruction via multichannel singular spectrum analysis," *Geophysics*, vol. 76, no. 3, pp. 25–32, 2011.
[17] Y. Chen, W. Huang, D. Zhang, and W. Chen, "An open-source MATLAB code package for improved rank-reduction 3D seismic data denoising and reconstruction," *Comput. Geosci.*, vol. 95, pp. 59–66, Oct. 2016.
[18] J. Gao, Z. Li, M. Zhang, Y. Gao, and W. Gao, "Unsupervised seismic random noise suppression based on local similarity and replacement strategy," *IEEE Access*, vol. 11, pp. 48924–48934, 2023.
[19] C. Liang, H. Lin, and H. Ma, "Reinforcement learning-based denoising model for seismic random noise attenuation," *IEEE Trans. Geosci. Remote Sens.*, vol. 61, pp. 1–17, 2023, Art. no. 5908217.
[20] W. Zhu, S. M. Mousavi, and G. C. Beroza, "Seismic signal denoising and decomposition using deep neural networks," *IEEE Trans. Geosci. Remote Sens.*, vol. 57, no. 11, pp. 9476–9488, Nov. 2019.
[21] X. Dong, J. Lin, S. Lu, X. Huang, H. Wang, and Y. Li, "Seismic shot gather denoising by using a supervised-deep-learning method with weak dependence on real noise data: A solution to the lack of real noise data," *Surv. Geophys.*, vol. 43, no. 5, pp. 1363–1394, 2022.
[22] J. Li, X. Wu, and Z. Hu, "Deep learning for simultaneous seismic image super-resolution and denoising," *IEEE Trans. Geosci. Remote Sens.*, vol. 60, pp. 1–11, 2022, Art. no. 5901611.
[23] X. Dong, T. Zhong, and Y. Li, "A deep-learning-based denoising method for multiarea surface seismic data," *IEEE Geosci. Remote Sens. Lett.*, vol. 18, no. 5, pp. 925–929, May 2021.
[24] R. Tibi, P. Hammond, R. Brogan, C. J. Young, and K. Koper, "Deep learning denoising applied to regional distance seismic data in Utah," *Bull. Seismological Soc. Amer.*, vol. 111, no. 2, pp. 775–790, 2021.
[25] Q. Feng and Y. Li, "Denoising deep learning network based on singular spectrum analysis—DAS seismic data denoising with multichannel SVDDCNN," *IEEE Trans. Geosci. Remote Sens.*, vol. 60, pp. 1–11, 2022, Art. no. 5902911.
[26] J. Gao, Z. Li, and M. Zhang, "Seismic random noise attenuation based on m-resunet," *IEEE Trans. Geosci. Remote Sens.*, vol. 61, pp. 1–16, 2023, Art. no. 5913716.
[27] B. Liu, J. Yue, Z. Zuo, X. Xu, C. Fu, S. Yang, and P. Jiang, "Unsupervised deep learning for random noise attenuation of seismic data," *IEEE Geosci. Remote Sens. Lett.*, vol. 19, pp. 1–5, 2022.
[28] T. Zhong, M. Cheng, X. Dong, Y. Li, and N. Wu, "Seismic random noise suppression by using deep residual U-Net," *J. Petroleum Sci. Eng.*, vol. 209, Feb. 2022, Art. no. 109901.

JIAN GAO received the B.S. degree in transportation from Inner Mongolia University, Hohhot, China, in 2020. He is currently pursuing the M.S. degree in geophysics with China University of Petroleum (East China).

His research interests include deep learning, swarm intelligence, and seismic data denoising and reconstruction.

YIXUAN GAO is currently pursuing the B.S. degree in biological science with Qufu Normal University.

Her research interests include swarm intelligence and deep learning.

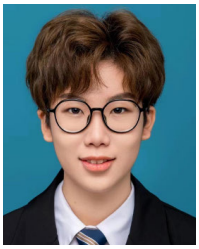

WANYUE GAO is currently pursuing the B.S. degree in logistics with Shandong Normal University.

Her research interests include supply chain management and deep learning.